Single-photon emission tomographic quantification in spherical objects: effects of object size and background

Felicia Zito, Maria Carla Gilardi, Patrizia Magnani and Ferruccio Fazio

INB-CNR, University of Milan, Institute H San Raffaele, Milan, Italy

Received 24 May and in revised form 4 October 1995

Abstract. A method was set up for single-photon emission tomographic (SPET) quantification of radioactivity concentration in small anatomical structures. The method is based on the theoretical model proposed by Kessler et al. (*J. Comput Assist Tomogr* 1984; 8: 514–522) describing the effects of spatial resolution (partial volume effect and spillover) on the quantification of radioactivity concentration in small spherical objects. The model was validated here in SPET, by phantom experimental measurements, in relation to object size and source/background contrast. Good agreement was found between model-predicted and SPET-measured radioactivity concentration ratios in hot spots in hot background experiments. Accuracy of the method was assessed for comparison of model-corrected and true radioactivity concentration ratios and was found to be within 8.5% over the full range of object size (9.4–36.5 mm). The good agreement found indicates that the model can be used to correct for partial volume effect and spillover in specific clinical situations, when the anatomical structure under study can be approximated by a sphere of known size (e.g. neuroreceptor and tumour studies). The method was applied to a representative SPET monoclonal antibody patient study for the quantification of radioactivity concentration in ocular melanoma.

Key words: Single-photon emission tomography – Partial volume effect – Spillover – Recovery coefficient

Eur J Nucl Med (1996) 23:263–271

Introduction

Single-photon emission tomography (SPET) imaging provides better anatomical localization and higher contrast than planar scintigraphy and as a consequence offers the potential for quantitative assessment of volume and radioactivity concentration in organs and lesions. Quantification can be useful in facilitating diagnosis [1–4] as well as for therapeutic purposes [5], such as in the estimation of dose to tumour and normal tissues.

The attenuation of primary photons, the undesired detection of scattered radiation and the finite spatial resolution of the imaging tomographic system are physical factors affecting the accuracy of quantification in SPET. In particular the limited spatial resolution of the technique causes an underestimation of the radioactivity concentration in small structures, the extent of this effect being related to the shape and size of the source object under study. This low quantitative accuracy is in fact dependent on the combined effect of system spatial resolution, radioactivity contrast between the source object and the surrounding background, and the image noise level [6].

In this work a theoretical model proposed by Kessler et al. [7] describing the effects of spatial resolution on the quantification of radioactivity concentration in small spherical objects was adopted. The model, originally developed for positron emission tomography (PET), was validated here in SPET by phantom experimental measurements in relation to object size and lesion/background contrast. The method was applied to a representative SPET monoclonal antibody patient study for the quantification of radioactivity concentration in ocular melanoma.

Theory

In the quantification of the radioactivity concentration in small spherical radioactive sources surrounded by a uniform radioactive background, quantification accuracy is influenced by effects related to the spatial resolution of the system:

1. Partial volume effect, resulting in an underestimation of the measured concentration in the small sources
2. Spillover from the surrounding background, erroneously increasing the estimate of measured concentration.

A theoretical model was proposed by Kessler et al. [7] to describe in PET "the recovery of activity from objects having limited size and differing contrast". The model assumes a gaussian system point spread function to describe system spatial resolution and handles image counts distribution as a linear system.

Correspondence to: F. Fazio, Department of Nuclear Medicine, Institute H San Raffaele, via Olgettina 60, I-20132 Milano, Italy

According to the model, given a sphere of uniform radioactivity concentration Cs and radius r, surrounded by a uniform background C_b, measured counts in the sphere can be predicted as:

$$C_{sp}(r, C_s, C_b)=C_s \cdot F(r)-C_b \cdot F(r)+C_b$$
$$C_{sp}(r, C_s, C_b)=C_s \cdot F(r)+C_b \cdot [1-F(r)], \quad (1)$$

$F(r)$ being the integral of a symmetric gaussian weighting function over the radioactive source distribution.

In Eq. 1 the first term accounts for partial volume effect, while the second accounts for the effect of spillover. The effect of partial volume and spillover can be experimentally determined by distinct measurements in the simplified cases of hot spheres in a cold background ($C_b=0$) and of cold spheres in a hot background ($C_s=0$) respectively.

To quantify partial volume effect, hot spot recovery coefficients (RC_H) can be derived for radioactive spheres in a cold background as the ratio between measured and true radioactivity concentrations. According to Eq. 1:

$$RC_H=C_{sp}(r, C_s, C_b=0)/C_s=F(r). \quad (2)$$

To quantify spillover, cold spot recovery coefficients (RC_C) can be defined for cold spheres in a radioactive background as the ratio between apparent sphere and background radioactivity concentration. According to Eq. 1:

$$RC_C=C_{sp}(r, C_s=0, C_b)/C_b=[1-F(r)]. \quad (3)$$

For a given system spatial resolution, both RC_H and RC_C are dependent on the shape and size of the source objects. Furthermore, according to Eqs. 1–3:

$$RC_C=1-RC_H \quad (4)$$

In the case of radioactive objects in a radioactive background, based on Eqs. 2 and 3, Eq. 1 can be rewritten as:

$$C_{sp}(r, C_s, C_b)=C_s \cdot RC_H+C_b \cdot RC_C. \quad (5)$$

According to this model, neglecting scatter contribution, the radioactivity concentration measured by SPET in a small anatomical structure (C_{sm}), surrounded by a uniform radioactive background (C_{bm}), can be corrected for partial volume effect and spillover by rearranging Eq. 5:

$$C_s^*=(C_{sm}-C_{bm} \cdot RC_C)/RC_H=C_{sm}/RC_H-C_{bm}/RC_H+C_{bm}. \quad (6)$$

The application of Eq. 6 assumes that (a) the object size is known, (b) RC_H/RC_C values are known as a function of the object size and (c) an accurate SPET estimate of the background is available.

Materials and methods

Data acquisition and reconstruction

A brain-dedicated SPET system, CERASPECT (D.S.I., Waltham, Mass., USA) [8], equipped with a high-resolution parallel hole collimator, was used to acquire tomographic data. The system has a field of view of 21 cm transaxially and 10.5 cm axially. The detailed physical performance of the system has been described elsewhere [9, 10]. Data were sampled using 120 (×3°) angular steps covering 360°, with a pixel size of 0.164 cm (corresponding to a projection matrix size of 128×64). For all acquisitions the count rate was less than 4000 cps in order to ensure a count rate loss within 5%.

Tomographic slices of all studies were reconstructed according to the protocol used for clinical brain studies. In particular, projection data were corrected for physical decay of ^{99m}Tc, then prefiltered with a bidimensional Hann filter with a cutoff equal to 0.5 Nyquist frequency and reconstructed using a filtered back-projection algorithm with a ramp filter. Attenuation correction was performed by the Chang method [11] with constant attenuation coefficient μ. A μ value of 0.1 cm^{-1} was used, lower than the theoretical value of μ=0.15 cm^{-1} for technetium-99m in water, in order to compensate for scatter [12].

System spatial resolution, defined as the full width at half maximum (FWHM) of the line spread function, measured by a line source in water on axis and 5 cm off axis, was 10.6 mm and 10.0 mm, respectively (average of radial and tangential values).

Data were reconstructed on 64 contiguous slices (one pixel thick) on 128×128 matrices, resulting in a cubic voxel (0.164×0.164×0.164 cm^3).

Phantom studies

To simulate small structures inside the head, six fillable perspex spheres with a wall thickness of 1.6 mm and internal diameters of 9.4 mm (L1), 13.0 mm (L2), 15.5 mm (L3), 22.0 mm (L4), 28.0 mm (L5) and 36.5 mm (L6) contained in a cylindrical phantom (20 cm diameter, 12 cm height) and mounted internally at a radial distance of 5 cm from the centre (one-half the radius) were used for all experiments. The spheres were arranged to have equators at the same level. The true volumes of the spheres were mathematically calculated by knowledge of internal diameters and verified by the difference in mass between water-filled and empty spheres. The cylindrical phantom was positioned with the long axis coincident with the axis of rotation of the imaging system.

For all experiments, phantoms were filled with a homogeneous solution of ^{99m}Tc. For each different solution, the specific radioactive concentration (KBq/ml) was measured with a calibrated well counter using withdrawn samples of 1 ml.

Hot spots in a cold background. All six spheres were filled with the same radioactive solution (120 KBq/ml) (hot spots) and then inserted into the cylindrical phantom filled with water (cold background).

Cold spots in a hot background. The six spheres, filled with water (cold spots), were inserted into the cylindrical phantom containing a uniform radioactive solution (37 KBq/ml) (hot background). About 600 kcounts/slice were collected.

Hot spots in a hot background. A radioactive solution of 37 KBq/ml was used to fill the cylindrical phantom (hot background). The six spheres (hot spots) were filled 3 times with three different radioactive solutions to produce hot sphere/hot background concentration ratios (R) of 5.9, 3.2 and 1.9 respectively. For each of the three conditions, five independent measurements were repeated, collecting approximately 250 kcounts/slice in each study.

Table 1. List of abbreviations used in phantom studies

C_S	True sphere radioactivity concentration assessed by the well-counter
C_{sp}	Predicted sphere radioactivity concentration according to the model
C_{sm}	SPET-measured sphere radioactivity concentration
C_s*	Model-corrected sphere radioactivity concentration
C_b	True background radioactivity concentration assessed by the well-counter
C_{bm}	SPET-measured background radioactivity concentration
RC_H	Hot spot recovery coefficient
RC_C	Cold spot recovery coefficient
R	True sphere/background radioactivity concentration ratio
R_p	Predicted sphere/background radioactivity concentration ratio
R_m	SPET-measured sphere/background concentration ratio

Cross-calibration

The cylindrical container (the same as was used to mount the spheres) filled with a uniform radioactive solution of ^{99m}Tc was scanned. Sixty-four transaxial slices of the cylindrical phantom were reconstructed as previously described. Count density (cps/voxel) was measured in each slice by drawing a circular region of interest (ROI) with a diameter covering 80% of the effective diameter of the phantom, thus ensuring a uniform counts distribution, excluding edge effects. Mean count density was calculated by averaging over the 64 slices. This was divided by the well-counter measured radioactivity concentration to obtain a cross-calibration factor K as (cps/voxel)/(KBq/ml).

Data analysis

For all phantom experiments, reconstructed transaxial slices were divided pixel by pixel by the cross-calibration factor K so that image counts in each voxel could be expressed in absolute radioactive concentration (KBq/ml). Various parameters were calculated and the abbreviations used are listed in Table 1.

Hot spot recovery coefficients. Hot spot recovery coefficients (RC_H) were determined as the ratio between the SPET-measured (C_{sm}) and the true well-counter estimated (C_s) activity concentration in each sphere:

$$RC_H=C_{sm}/C_s.$$

C_{sm} was assessed as the mean value in a circular ROI (three pixels diameter), drawn on the centre of each sphere, using the transaxial slice crossing th spheres' equator.

Transaxial slices (~34) covering the whole set of six spheres were added together; circular ROIs were defined, with the diameter approximately equal to the size of the sphere plus 2 FWHM. Total activity in each sphere was thus measured by SPET and compared to the true value.

Cold spot recovery coefficients. Cold spot recovery coefficients (RC_C) were predicted as complementary to RC_H values according to Eq. 4.

Measured RC_C values were determined as the ratio between the apparent measured radioactivity concentration in the non-radioactive spheres (C_{sm}) and the measured concentration in the surrounding background (C_{bm}):

$$RC_C=C_{sm}/C_{bm}.$$

C_{sm} was mearued as in the hot spots in a cold background experiment. C_{bm} was assessed as the mean radioactivity concentration in a large irregular ROI drawn on the background, excluding cold spot regions.

Validation of the model in the hot spots in a hot background experiment. The model was validated by comparing the model-predicted and the SPET-measured sphere/background radioactivity concentration ratio in the hot spots in a hot background experiment.

Apparent radioactivity concentration in a sphere, C_{sp}, was predicted according to Eq. 5, RC_H and RC_C being the measured recovery coefficients for the hot and cold spot situations and C_s and C_b, the true well-counter measured sphere and background radioactivity concentration respectively. Predicted ratios (R_p) of radioactivity concentration in the hot spots and in the background were estimated as:

$$R_p=C_{sp}/C_b.$$

For the three R conditions, in each of the five SPET studies performed, radioactivity concentrations in the spheres (C_{sm}) and in the background (C_{bm}) were measured as in the previous experiments. Measured ratios (R_m) were estimated as:

$$R_m=C_{sm}/C_{bm}.$$

Average values of R_m and standard deviations were calculated over the five SPET experiments.

Accuracy of the model. Accuracy of the model was estimated as the percentage error between measured and true sphere/background radioactivity concentration ratio, by using SPET data of the hot spots in a hot background experiment.

Radioactivity concentration in the spheres was compensated for both partial volume effect and spillover according to Eq. 6 and the percentage errors were estimated as:

$$\varepsilon^*=100\cdot[C_s^*/C_{bm}-R]/R.$$

For comparison, the percentage errors when no compensation for partial volume effect and spillover was performed (ε) and when only partial volume effect was accounted for (ε°) were calculated:

$$\varepsilon=100\cdot[C_{sm}/C_{bm}-R]/R$$
$$\varepsilon^\circ=100\cdot[(C_{sm}/RC_H)/C_{bm}-R]/R.$$

Patient study

A patient presenting with ocular melanoma was considered as a representative case. Informed written consent was obtained for the study.

The tumour shape was approximated to a sphere and the diameter was assessed by CT scan.

As part of the diagnostic protocol, independent of the present work, two immunoscintigraphic (ISG) SPET studies were performed, according to a conventional ISG method [13] and to the three-step ISG method [14]. In the first study, ~20 mCi of ^{99m}Tc-labelled anti-melanoma monoclonal antibodies (MoAb 225.28S) was administered and the scan was performed about 6 h after injection. In the three-step ISG study, according to the pre-targeting model, anti-melanoma MoAbs were first injected i.v., followed 24 h later by avidin administration and 48 h later by i.v. injection of ~20 mCi of [^{99m}Tc]PnAO-biotin. The SPET study was performed 2.5 h afterwards. This last approach presents faster clearance of radioactivity from the blood, thus resulting in an improved lesion/background radioactivity ratio. SPET acquisition, reconstruction and calibration procedures were as previously described.

In both studies, radioactivity concentration in the ocular melanoma (T) was measured by drawing a circular ROI (three pixels diameter) on the most representative SPET slice, containing the maximum pixel value in the lesion. Radioactivity concentration in the surrounding background was estimated by drawing a circular ROI (eight pixels diameter) on the healthy contralateral orbit (B). T and B were decay corrected at the injection time. Both of these SPET studies, by approximating the tumour mass to a spherical structure, could be analysed as a hot spots in a hot background situation.

Radioactivity concentration in the tumour was assessed as follows:

1. Estimate of the radioactivity concentration in the tumour (T) with no compensation for partial volume effect and spillover.
2. Estimate of radioactivity concentration in the tumour with compensation for partial volume effect, neglecting the surrounding background ($T°$):

$T°=T/RC_H$,

RC_H being the recovery coefficient estimated for a sphere of diameter equivalent to the lesion size normalized by the appropriate FWHM (system spatial resolution measured at the same lesion position).
3. Estimate of radioactivity concentration in the tumour, with compensation for both partial volume effect and spillover, accounting for the surrounding background ($T*$). According to the theoretical model (Eq. 6):

$T*=T/RC_H-B/RC_H+B$.

Lesion/background ratios (T/B, $T°/B$, $T*/B$) were also calculated.

Results

Phantom studies

Hot spot recovery coefficients

A transaxial slice of the hot spots in a cold background experiment, crossing the spheres' equator, is shown in Fig. 1a. Although all spheres were filled with the same radioactive concentration, underestimation in the smaller objects is evident, as a result of partial volume effect. This effect is quantified in terms of recovery coefficients (RC_H), which represent the percentage of radioactivity concentration recovered by SPET. RC_H values are plotted in Fig. 1b versus the sphere diameter, normalized to the system FWHM. RC_H values increase with the object size, reaching a plateau (RC_H=0.9) for a sphere diameter equal to approximately 3 times the FWHM (30 mm). For the sphere of 9.4 mm internal diameter (~1 FWHM) RC_H is 23%, proving a strong underestimation of radioactivity concentration. 100% recovery (RC_H=1) is never obtained, even for the largest sphere. This effect can be attributed to the approximate scatter correction method used. Different scatter components are in fact expected for different source distributions, and the cross-calibration factor K, calculated by a uniform radioactive cylinder, is overestimated when used for the hot spots in a cold background experiment, explaining the underestimation of RC_H values. A similar effect was observed in PET [15, 16]. The overestimated K factor can also explain the systematic underestimation (within 12%) of measured versus true calculated total activity in the spheres (Table 2). Measured activity was in fact assessed in each sphere by a large ROI and all counts spread around the sphere were supposed to be included [17].

Table 2. Hot spots in a cold background experiment. Comparison of SPET-measured and true total radioactivity present in the spheres

Sphere	D/FWHM	Measured activity (MBq)	True activity (MBq)
L6	3.65	2.93	3.07
L5	2.80	1.24	1.39
L4	2.20	0.59	0.67
L3	1.55	0.21	0.24
L2	1.30	0.12	0.13
L1	0.94	0.05	0.05

Cold spot recovery coefficients

A transaxial slice of the cold spots in a hot background experiment, crossing the spheres' equator, is shown in Fig. 2a. Although the spheres are filled with non-radio-

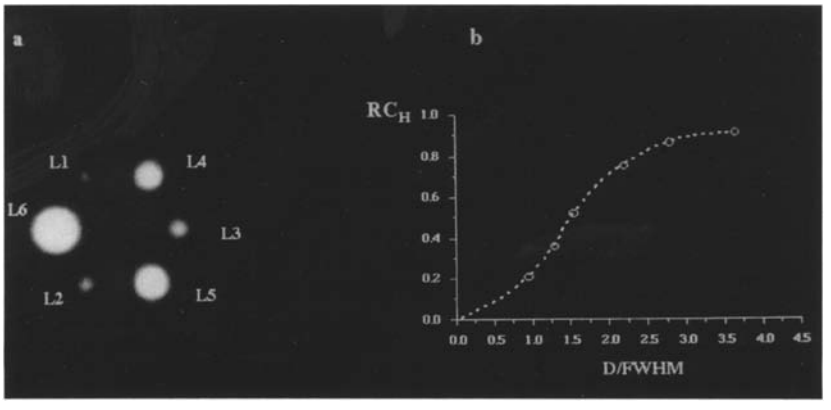

Fig. 1a, b. Hot spots in a cold background experiment. **a** Representative SPET cross-sectional image showing the apparent decrease in radioactivity concentration as a function of the sphere size, as a result of the partial volume effect. **b** Hot spot recovery coefficient (RC_H) values as a function of sphere diameter (D), normalized to system FWHM. The curve is extrapolated to zero using a cubic function

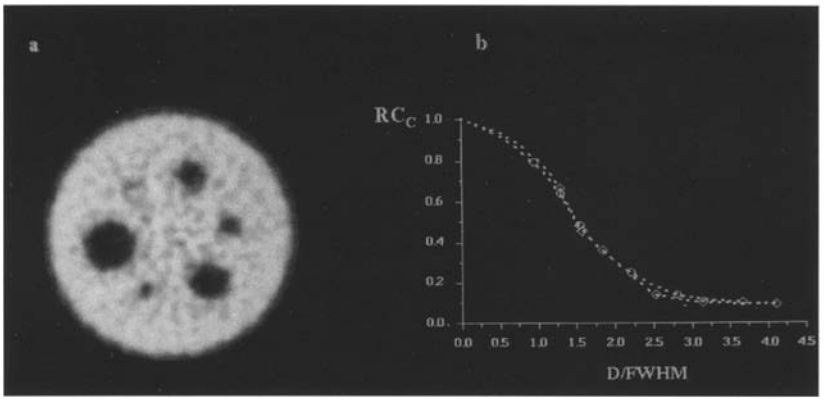

Fig. 2a, b. Cold spots in a hot background experiment. **a** Representative SPET cross-sectional image showing the apparent radioactivity concentration in the spheres, as a result of scatter and spillover from the surrounding background. **b** Model-predicted (–○–) and SPET-measured (–◇–) cold spot recovery coefficient (RC_C) values as a function of sphere diameter (D), normalized to system FWHM. Curves are extrapolated to 1 using a cubic function

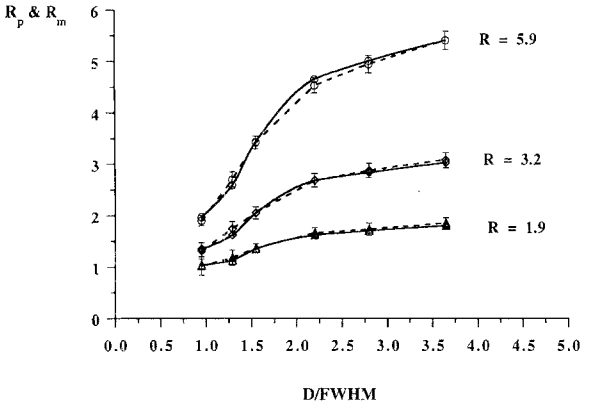

Fig. 3. Hot spots in a hot background experiment. Model-predicted R_p (*solid line*) and SPET-measured average R_m (*dotted line*) radioactivity concentration ratios, as a function of sphere size normalized to system FWHM, for the three contrast levels, R=5.9 (○), R=3.2 (◇) and R=1.9 (△). For each R_m value *error bars* representing 1 standard deviation are shown

active water, apparent activity in the spheres can be observed as a result of scatter and spillover. RC_C values describe the influence of the hot background on the cold spheres. RC_C values are plotted in Fig. 2b versus the sphere diameter, normalized for the system FWHM. RC_C values increase by decreasing the object size. For the sphere L1 (external diameter=1.3 FWHM), RC_C was 0.66, meaning that 66% of the radioactivity concentration in the background was incorrectly measured in the small sphere.

Calculated RC_C values, complementary to RC_H values, are also shown in Fig. 2b. Good overall agreement between measured and calculated RC_C values can be observed. This result represents a validation of Kessler's theory in modelling the relationship between partial volume effect and spillover. Furthermore, the validity of such a relation allows RC_H and RC_C to be derived by a single experiment.

Validation of the model

R_p and R_m values, representing the model-predicted and the SPET-measured ratio between the radioactivity concentration in the spheres (C_{sp}, C_{sm}) and the background (C_b, C_{bm}), are plotted in Fig. 3 for the three contrast levels, as a function of object size, normalized to the system FWHM.

For all three R ratios, a good statistical association ($r^2 \geq 0.99$, $P<0.001$) was found between R_p and R_m values using a linear regression analysis. Such a good agreement proves the validity of the model in predicting radioactivity concentration, accounting for partial volume effect and spillover.

As expected in the case of hot spots, R_p and R_m values decrease when the size of the spheres is decreased, because C_{sp} and C_{sm} are underestimated as a result of the partial volume effect. It can also be observed that the same R_p/R_m value is measured for different R ratios in correspondence to different object sizes. For example, a

Table 3. Percentage errors estimated between measured and true radioactivity concentration ratios for the three contrast levels "R". ε: no compensation applied; ε°: only partial volume effect corrected; ε*: correction for both partial volume effect and spillover according to the model

	R=5.9			R=3.2			R=1.9		
	ε	ε°	ε*	ε	ε°	ε*	ε	ε°	ε*
L6	− 8.4	1.8	0.1	− 5.5	5.0	1.9	− 2.5	8.4	3.1
L5	−16.3	− 0.4	−2.8	−11.7	5.1	0.7	− 8.7	8.6	1.1
L4	−21.2	1.0	−5.0	−17.5	5.7	−0.6	−12.7	12.0	1.2
L3	−42.0	11.5	−0.3	−36.9	21.3	0.0	−27.8	38.9	2.5
L2	−54.2	27.1	5.0	−46.5	48.7	8.5	−37.7	72.9	4.2
L1	−67.8	40.0	−5.0	−59.7	75.3	−6.4	−46.3	133.6	−6.0

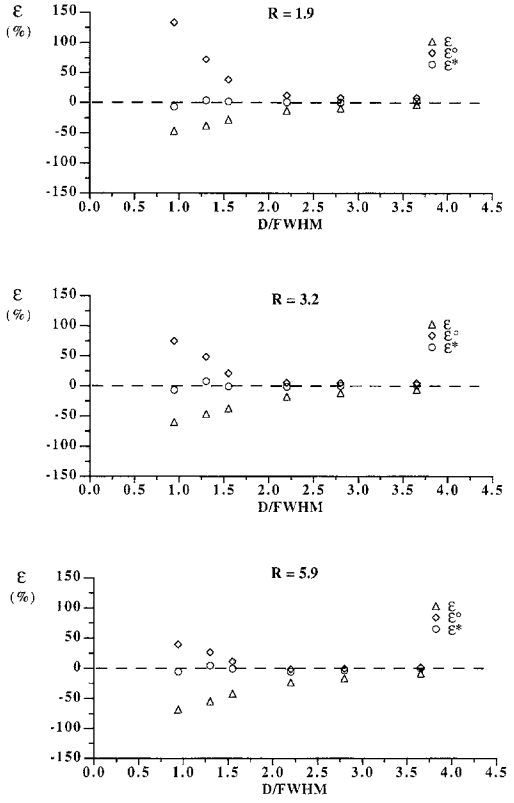

Fig. 4. Percentage errors estimated between measured and true radioactivity concentration ratios, when no compensation is applied (ε), when only partial volume effect is corrected (ε°) and accounting for both partial volume effect and spillover according to the model (ε*)

ratio of ~2 is measured for L1 at R=5.9 and for L3 at R=3.2, and a ratio of ~1.7 is measured for L2 at R=3.2 and for L5 at R=1.9. Due to this non-univocal relationship between radioactivity concentration ratio and object size, quantitative assessment of radioactivity concentration in clinical images is not possible unless the size of the object is known, thus allowing recognition of the true R ratio and compensation for the dependence on the object size.

Accuracy of the model

For the three contrast levels, percentage errors estimated between SPET-measured radioactivity concentration ratios (R_m) and true ratios (R) in the cases of compensation for both partial volume effect and spillover (ε*), compensation for partial volume effect only (ε°) and no compensation for the effects of spatial resolution (ε) are reported in Table 3 and plotted in Fig. 4 as a function of object size normalized to the system FWHM.

The small ε* values (in the range −6%–8.5%) observed for all three R levels and over the full range of object size prove the accuracy of the model in compensating for both partial volume effect and spillover and thus in quantifying radioactivity concentration.

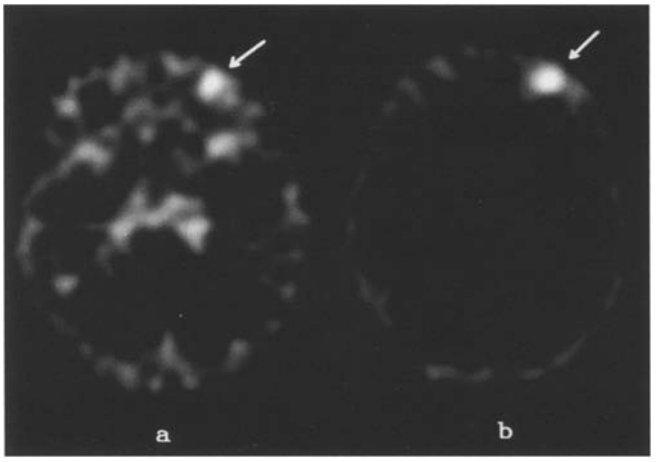

Fig. 5a, b. SPET images of a patient presenting with ocular melanoma (*arrows*). **a** Conventional ISG study. **b** Three-step ISG study. (See text for explanations)

When only partial volume effect was corrected, positive ε° values were found, indicating an overestimation of the radioactivity concentration. This is the result of spillover, its effect being stronger for lower R ratios and for small objects. In particular, for a sphere size smaller than twice the system spatial resolution, a fast increase in ε° values could be observed.

When no compensation for partial volume effect and spillover was performed, negative ε values were found as a result of the partial volume effect dominating over spillover. However, due to the artificial increase in radioactivity concentration induced by spillover, underestimation was less relevant for low R ratios. For sphere diameters smaller than twice the system spatial resolution, absolute ε values increased, although less rapidly than ε° values.

From these data it appears that accurate results can be obtained if both partial volume effect and spillover are compensated according to Kessler's model. If spillover is not taken into account, in the case of objects smaller than twice the spatial resolution, smaller errors are found by neglecting partial volume effect and avoiding any correction.

Patient study

Figure 5 shows representative images of the conventional ISG and the three-step ISG SPET patient study respectively. The improved lesion/background ratio in the three-step ISG method is visually evident.

For a structure of diameter 9.7 mm, as estimated by CT scan, an RC_H of 0.25 was interpolated from Fig. 1b, accounting for the appropriate FWHM (9.7 mm) at the lesion position (6.5 cm off axis). Table 4 summarizes quantitative data in terms of absolute radioactivity concentration and lesion/background radioactivity concentration ratio obtained applying different corrections for

Table 4. Immunoscintigraphic SPET patient data relative to the conventional ISG and three-step ISG studies. Tumour radioactivity concentration and lesion/background radioactivity concentration ratio without compensation for spatial resolution (*T, T/B*), with compensation for partial volume effect (T°,T°/B) and with compensation for partial volume effect and spillover according to the model (T^*,T^*/B)

	T (KBq/ml)	T° (KBq/ml)	T^* (KBq/ml)	T/B	T°/B	T^*/B
ISG	16.45	66.60	43.29	2.00	8.20	5.30
Three-step ISG	18.50	74.00	57.35	3.20	12.90	10.00

geometrical factors and background level. When no compensation was applied, an underestimation of 61% and 67% was found in the tumour radioactivity concentration T with respect to T^* in the ISG and three-step ISG studies, respectively. Compensating only for partial volume effect, an overestimation of 52% and 19% for the ISG and three-step ISG methods was found in T° with respect to T^*.

Lesion/background contrast was also affected by partial volume and spillover and the accuracy in its estimation was dependent on the correction applied (Table 4). In the case of no compensation and when only partial volume effect compensation was applied, a contrast improvement equal to 1.6 for the three-step ISG over the conventional ISG method was found. This improvement increased to 1.9 when accounting for both partial volume effect and spillover, according to the model.

Discussion

The effects of spatial resolution on SPET and PET images have been widely discussed and the need for compensation for such effects has been demonstrated, when accurate measurements of radioactivity concentration are desired [6, 7, 15–23].

A simple description of the effect of spatial resolution on PET images was proposed by Kessler et al. [7]. According to this model, measured concentration in spherical objects surrounded by a uniform background can be expressed as the sum of two contributions: the radioactivity in the sphere decreased by the spreading effect of spatial resolution out of the sphere (partial volume effect) and the radioactivity in the background, spread into the sphere (spillover). Partial volume effect and spillover can be quantitatively estimated in terms of recovery coefficients measured in the two extreme situations of radioactive spheres in a non-radioactive background (RC_H) and non-radioactive spheres in a radioactive background (RC_C). Once RC_H/RC_C values are known, if a good estimate of the background radioactivity can be performed, measured radioactivity concentration in the spheres can be corrected for partial volume effect and spillover.

This model, originally developed with reference to PET cerebral images representing regional blood flow or glucose metabolism, today appears particularly applicable in neuroreceptor or tumour SPET studies, where basal ganglia and some tumours, respectively, can be approximated by spherical structures. The model can therefore represent a simple and powerful tool for the quantification of tracer uptake in such studies, performed by either PET or SPET.

The aim of the present work was to verify the validity of the model described and to assess its accuracy, in relation to object size and contrast. The study focussed on spherical objects. In particular, spheres of different internal diameters, ranging from 9.4 to 36.5 mm to simulate anatomical structures, were positioned in a cylindrical phantom, simulating the head. Radioactivity concentrations in the spheres and in the phantom were varied to simulate different radioactive contrast levels.

Acquisition and reconstruction parameters and procedures typical of clinical studies were adopted. In particular the Chang attenuation correction method with an underestimated attenuation coefficient to compensate for scatter was used. The μ value of 0.1 cm^{-1} was determined to compensate scatter in a uniform 20-cm cylinder. However, this approximate scatter correction technique does not properly account for different scatter components present in different source distributions (e.g. hot spheres in a cold background). This results in an overestimation of the cross-calibration factor K (assessed with a 20-cm uniform cylindrial phantom), when used to quantify radioactivity in spherical objects. This explains the underestimation of the recovery coefficients and of the integral radioactivity in the hot spheres in a cold background. A more accurate scatter compensation method should be used to account for the ~10% inaccuracy found throughout the work.

RC_H and RC_C coefficients were measured as a function of the object size, normalized by the system spatial resolution (FWHM) at 5 cm off axis (where the spheres were located). This normalization accounts for the variation of spatial resolution [17], which in particular for SPET is dependent on the position of source from the centre.

Typical behaviour for recovery coefficients (RC_H, RC_C) versus object size was found, showing that accurate results without compensation for spatial resolution can be obtained for objects greater in size than approximately 3 times the system spatial resolution (3 FWHM=30 mm). For smaller object sizes, partial vol-

ume effect and spillover can significantly affect SPET quantification. As an example, in a radioactive structure of ~1 FWHM diameter, an underestimation of up to 75% in the assessment of radioactivity concentration can occur due to the partial volume effect.

A good agreement was observed between RC_C values predicted as complementary to RC_H according to Kessler's theory and those measured by SPET.

The model was validated at different contrast levels in the hot spots in a hot background SPET studies, by comparing model-predicted R_p and measured R_m sphere/background radioactivity concentration ratios (Fig. 3). The excellent agreement between R_p and R_m (r^2>0.99) proves the ability of the model in describing the combined effect of partial volume and spillover.

The accuracy of the model in compensating for such effects was also evaluated by comparing R_m values with the true sphere/background radioactivity concentration ratios R (Table 3, Fig. 4). Percentage errors within 8.5% were found for all contrast levels and in the full range of object size. Large errors were observed, in particular for spheres with diameter smaller than twice the system FWHM, when no compensation or only correction for partial volume effect was performed.

The effect of spillover was shown as an artificial increase in radioactivity concentration in the spheres, particularly for small objects and low contrast levels, partially compensating the underestimation due to the partial volume effect.

SPET immunoscintigraphic data from a representative patient presenting with an ocular melanoma were analysed. Errors greater than 50% in the estimation of the radioactivity concentration in the tumour were found when both the effect of partial volume and that of spillover were not compensated (T and $T°$ vs $T*$), proving the need to take spatial resolution correctly into account when quantifying SPET data (Table 4). In radiotherapeutic applications, such large errors in the estimate of the radioactivity concentration in the tumour would affect the efficacy of the therapy. Underestimation of the radioactivity concentration, as in the case of no corrections for the effects of spatial resolution, would result in an underestimation of the radiation dose to the tumour, thus leading to an increase in the injected radioactivity and consequent damage to healthy tissues. On the other hand, an overestimation of the radioactivity concentration, as in the case of correction for partial volume effect only, would lead to a reduction of the absorbed dose in the tumour, resulting in an ineffective therapy.

The estimate of the lesion/background ratio is also affected by spatial resolution, as shown by comparing T/B and $T°/B$ with the corrected $T*/B$ value for both the ISG and three-step ISG methods (Table 4). The different gain of lesion/background contrast in the three-step ISG method compared with the conventional ISG method, when applying the geometrical correction for partial volume effect (gain: 1.6) and when also compensating for spillover (gain: 1.9), indicates the importance of the correction applied even when semi-quantitative analyses of SPET data are performed in terms of the ratio between radioactivity concentrations in two anatomical structures.

The described procedure to compensate for the effect of spatial resolution could be extended to clinical studies involving tracers labelled with isotopes other than ^{99m}Tc (e.g. iodine-123 labelled neuroreceptor compounds or ^{201}Tl in brain tumour imaging) [3, 4, 24]. However, in these cases proper calibration is required to account for different scatter components and cross-calibration factors K, which are dependent on the physical characteristics of the isotope and the decay scheme.

Other considerations with regard to the validity of the model for clinical use are:

1. The model applies to spherical radioactive objects and was not validated for irregular structures. However, greater dependence of the effect of spatial resolution on the volume of the three-dimensional limited object than on its shape (cuboid, cylindrical, conic and spherical) has been described [22]. This supports the application of the considered model to anatomical structures which can be approximated by equivalent radius spheres [18].

2. The model refers to uniform radioactive distributions and quantitative accuracy for non-homogeneous sources is not evaluated.

3. The model was tested using good counting statistics images and noise effects on lesion detectability were neglected. However, statistical noise is important for the accuracy of quantification, and its combined effect with object size and contrast level is in fact worthy of consideration.

Other methods to compensate for the effect of spatial resolution have been proposed, either requiring registration of PET/SPET images to high-definition anatomical CT/MRI studies [19, 23] or based on specific assumptions, such as limited size of the structure only in one dimension (e.g. long infinite bar) [20]. The present method requires knowledge of the size of the anatomical structure under examination but no image fusion with CT/MRI is really needed. Furthermore, limited objects in three dimensions are considered, approximating an anatomical structure to a radioactive sphere surrounded by a uniform background.

In summary, the present work verifies the dependence of SPET quantitative accuracy on object size and lesion/background contrast. A simple and feasible method based on the model proposed by Kessler et al. [7] is presented and validated to improve the quantitative accuracy of SPET in specific clinical investigations such as tumour or neuroreceptor studies.

Acknowledgements. The authors wish to thank P. Garancini, C. Riddell and V. Bettinardi for their helpful discussions. This work was partially financed by Progetto Finalizzato Invecchiamento & Progetto Finalizzato ACRO-95 1774, CNR.

References

1. Burkard R, Kaiser KP, Wieler H, Klawki P, Linkamp A, Mittelbach L, Goller T. Contribution of thallium-201-SPECT to the grading of tumorous alterations of the brain. *Neurosurg Rev* 1992; 15: 265–273.
2. Paganelli G, Magnani P, Zito F, et al. Pre-targeted immunodetection in glioma patients: tumour localization and single-photon emission tomography imaging of [^{99m}Tc]PnAO-biotin. *Eur J Nucl Med* 1994; 21: 314–321.
3. Nadeau SE, Couch MW, Devane CL, Shukla SS. Regional analysis of D2 dopamine receptors in Parkinson's disease using SPECT and iodine-123-iodobenzamide. *J Nucl Med* 1995; 36: 384–393.
4. Laurelle M, Wallace E, Seibyl JP, Baldwin RM, Zea-Ponce Y, Zoghbi SS, Neumeyer JL, Charney DS, Hoffer PB, Innis RB. Graphical, kinetic, and equilibrium analysis of in vivo [^{123}I]β-CIT binding to dopamine transporters in healthy human subjects. *J Cereb Blood Flow Metab* 1994; 14: 982–994.
5. Kalofonos HP, Pawlikowska TR, Hemingway A, et al. Antibody guided diagnosis and therapy of brain gliomas using radiolabeled monoclonal antibodies against epidermal growth factor receptor and placental alkaline phosphatase. *J Nucl Med* 1989; 30: 1636–1645.
6. Gilland DR, Jaszczak RJ, Turkington TG, Greer KL, Coleman RE. Volume and activity quantification with Iodine 123 SPECT. *J Nucl Med* 1994; 35: 1707–1713.
7. Kessler RM, Ellis JR, Eden M. Analysis of emission tomographic scan data: limitations imposed by resolution and background. *J Comput Assist Tomogr* 1984; 8: 514–522.
8. Genna S, Smith AP. The development of ASPECT, an annular single crystal brain camera for high efficiency SPECT. *IEEE Trans Nucl Sci* 1988; NS-35: 654–658.
9. Zito F, Savi A, Fazio F. CERASPECT: a brain-dedicated SPECT system. Performance evaluation and comparison with the rotating gamma camera. *Phys Med Biol* 1993; 38: 1433–1442.
10. Bailey D, Zito F, Gilardi MC, Savi A, Fazio F, Jones T. Performance comparison of a state-of-the-art-neuro-SPECT scanner and a dedicated neuro-PET scanner. *Eur J Nucl Med* 1994; 21: 381–387.
11. Chang LT. A method for attenuation correction in radionuclide computed tomography. *IEEE Trans Nucl Sci* 1978; 25: 638–643.
12. Oppenheim BE. Scatter correction of SPECT. *J Nucl Med* 1984; 25: 928–929.
13. Bomanji J, Nimmon CC, Hungerford JL, Solanki K, Granowska M, Britton KE. Ocular radioimmunoscintigraphy: sensitivity and practical consideration. *J Nucl Med* 1988; 29: 1031–1044.
14. Paganelli G, Magnani P, Zito F, et al. Three-step monoclonal antibody tumor targeting in CEA-positive patients. *Cancer Res* 1991; 51: 5960–5966.
15. Spinks T, Guzzardi R, Bellina CR. Measurement of resolution and recovery in recent generation positron tomographs. *Eur J Nucl Med* 1989; 15: 750–755.
16. Bendriem B, Dewey SL, Schlyer DJ, Wolf AP, Volkow ND. Quantitation of the human basal ganglia with positron emission tomography: a phantom study of the effect of contrast and axial positioning. *IEEE Trans Med Imaging* 1991; 10: 216–222.
17. Hoffman EJ, Huang SC, Phelps ME. Quantitation in positron emission computed tomography: 1. Effect of objects size. *J Comput Assist Tomogr* 1979; 3: 299–308.
18. Mazziotta JC, Phelps ME, Plummet D, Kuhl DE. Quantitation in positron emission computed tomography: 5. Physical-anatomical effects. *J Comput Assist Tomogr* 1981; 5: 734–743.
19. Muller-Gartner HW, Links JM, Prince JL, Bryan RN, McVeigh E, Leal JP, Davatzikos C, Frost JJ. Measurement of radiotracer concentration in brain gray matter using positron emission tomography: MRI-based correction for partial volume effects. *J Cereb Blood Flow Metab* 1992; 12: 571–583.
20. Yu DC, Huang SC, Grafton ST, Melega WP, Barrio JR, Mazziotta CJ, Phelps ME. Methods for improving quantitation of putamen uptake constant of DOPA in PET studies. *J Nucl Med* 1993; 34: 679–688.
21. Kojima A, Matsumoto M, Takashi M, Hirota Y, Yoshida H. Effect of spatial resolution on SPECT quantification values. *J Nucl Med* 1989; 30: 508–514.
22. Alaamer AS, Fleming JS, Perring S. Evaluation of the factors affecting the accuracy and precision of a technique for quantification of volume and activity in SPECT. *Nucl Med Commun* 1994; 15: 758–771.
23. Videen TO, Perlmutter JS, Mintun MA, Raichle ME. Regional correction of positron emission tomography data for the effects of cerebral atrophy. *J Cereb Blood Flow Metab* 1988; 8: 662–670.
24. Kuikka JT, Tiihonen J, Bergstrom KA, Karhu J, Hartikainen P, Viinamaki H, Lansimies E, Lehtonen J, Hakola P. Imaging of serotonin and dopamine transporters in the living human brain. *Eur J Nucl Med* 1995; 22: 346–350.